Journal of Electron Spectroscopy and Related Phenomena 241 (2020) 146804

Contents lists available at ScienceDirect

Journal of Electron Spectroscopy and Related Phenomena

journal homepage: www.elsevier.com/locate/elspec

Spectra of correlated many-electron systems: From a one- to a two-particle description

Georg Rohringer

Russian Quantum Center, 143025 Skolkovo, Russia

ARTICLE INFO

Keywords:
Strong correlations
Quantum many-body techniques
Two-particle correlation functions

ABSTRACT

State-of-the-art spectroscopic techniques allow for a comprehensive understanding of one-electron excitations in various physically interesting and/or technologically relevant materials. While for weakly-correlated systems the corresponding one-particle spectral function $A(\omega, \mathbf{k})$ contains essentially all information about their physical properties the situation is much more complicated in the presence of strong electronic correlations. In fact, in the latter case different theoretical treatments often lead to very different explanations of the origin of specific features in the spectrum. A typical example is the pseudogap in the cuprates, i.e., the momentum-selective suppression of spectral weight at the Fermi level, which has been related to spin, charge or (d-wave) pairing fluctuations by different authors. This ambiguity about the underlying physical mechanism at work can be overcome by considering two-particle correlation functions as they are able to describe the collective modes of the system and can be also related to certain ground state properties. In this work, we will present different theoretical approaches for analyzing the spectrum of correlated systems by exploiting the information contained in these two-particle correlation functions. For the specific case of the pseudogap these procedures have allowed us (1) to identify antiferromagnetic spin fluctuations as microscopic origin of this spectral feature which (2) can be related to the formation of a resonating valence bond ground state in the system.

1. Introduction

Spectroscopic techniques are nowadays counted among the major experimental tools for the analysis of the electronic structure of solids. The common idea of these methods is to excite one or more electrons in a material which eventually leave the solid. Their energies and momenta provide important insights into the electronic structure of the system. Some of the most prominent representatives of this type of experimental techniques are the photoemission spectroscopy [1] (PES), its momentum-resolved counterpart [2] (angular resolved photoemission spectroscopy, ARPES) or scanning tunneling microscopy [3] (STM). They allow for an accurate determination of the *one-particle* electronic excitations and the Fermi surface of the material. For a correlated electron system, they also provide highly relevant information about the correlation effects between the particles.

On the theoretical side, results from PES, ARPES or STM experiments can be compared to the spectral function $A(\omega, \mathbf{k})$ which is obtained from the *one-particle Green's function* of the system. This quantity is determined by the crystallographic structure of the solid (which defines the band structure and the noninteracting density of states) and the correlation effects which are encoded in the so-called *self-energy*. The latter is responsible for strong coupling phenomena, such as the celebrated Mott–Hubbard metal-to-insulator transition (MIT) [4].

For a correlated system, the knowledge of the self-energy is unfortunately not sufficient for a comprehensive understanding of the physical processes which are responsible for certain features in the spectrum. A typical example is the momentum selective suppression of spectral weight – the so-called *pseudogap* – in the cuprates [5] or the nickelates [6] (for an example see Fig. 1). Despite the considerable efforts which have been undertaken both on the experimental as well as on the theoretical side in order to unravel the origin of this spectral feature, no consensus on this issue has been achieved so far. In fact, the pseudogap has been attributed by different groups to spin fluctuation [7–11], preformed pairs [12–16], Mottness [17,18], charge fluctuations [19–22] or Fermi-liquid scenarios [23].

In this paper, we review a number of theoretical methods [24–26], which allow us to identify the physical processes which are responsible for certain features in the self-energy. They are all based on the insight, that correlation effects in a many-electron system typically originate from the two-particle Coulomb repulsion between the electrons. Hence, the self-energy, which describes the correlation effects for a single particle which propagates through the material, must be determined by the sum of all its two-particle scattering events which are represented by the full two-particle scattering amplitude of the system. Formally,

E-mail address: grohringer@gmail.com.

https://doi.org/10.1016/j.elspec.2018.11.003
Received 3 July 2018; Received in revised form 4 October 2018; Accepted 6 November 2018
Available online 11 November 2018
0368-2048/

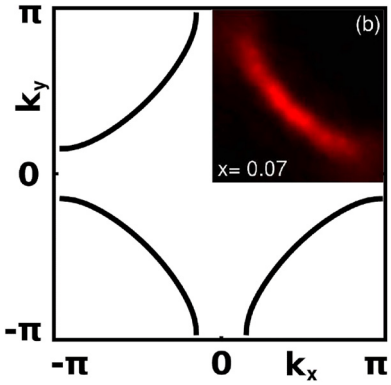

Fig. 1. Spectral function $A(\omega, \mathbf{k})$ of $La_{2-x}Sr_xCuO_4$ obtained from ARPES by Yoshida et al. [27] for $\omega = E_F$ as a function of k_x and k_y at a temperature $T = 20K$ and a hole doping of $x = 0.07$. The black lines indicate the Fermi surface. A large spectral weight (red) is found around the nodal point $\mathbf{k} = (\pi/2, \pi/2)$ while a strong suppression is observed at the antinodal point $\mathbf{k} = (0, \pi)$, which corresponds to a small and large value of $\Sigma(k)$, respectively. The figure has been readapted from Ref. [27].

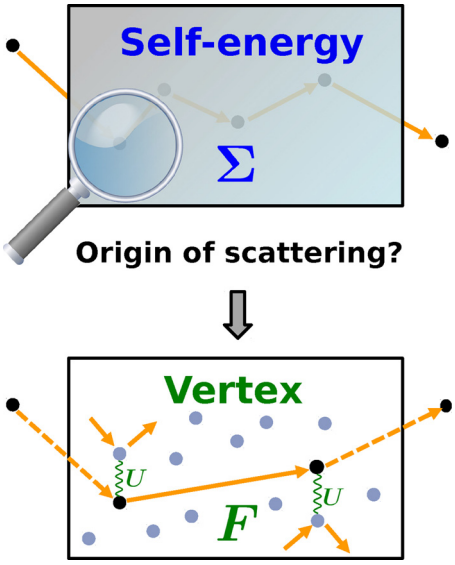

Fig. 2. Illustration of one-particle (G or Σ, upper panel) and two-particle ($G^{(2)}$ or F, lower panel) scattering amplitudes. The magnifying glass indicates that more insights into the effective one-particle scattering amplitude $\Sigma(k)$ can be obtained by analyzing the two-particle scattering events $F^{kk'q}_{\sigma\sigma'}$ from which the former originates.

such a relation is provided by the Dyson–Schwinger equation of motion (EOM) which we exploit to analyses how various two-particle processes contribute to the self-energy.

The paper is organized as follows: In Section 2 we introduce the formalism and define the relevant one- and two-particle correlation (vertex) functions which are required for our analysis and discuss their interconnection through the EOM. In Section 3, we present the general idea, how the EOM can be exploited to extract relevant information about the self-energy and discuss three theoretical approaches which are based on this conception. For each approach, we demonstrate its applicability by applying it to the above mentioned problem of the pseudogap in correlated electron systems. Finally, in Section 4 we conclude and discuss future experimental and theoretical perspectives for the application of the two-particle vertex functions.

2. One- and two-particle scattering processes

In this section, we present the fundamental concepts for the theoretical description of one- and two-particle scattering processes in many-electron systems. In particular, we will focus on the highly interesting situation where strong correlations between the particles prevail which makes independent electron descriptions, such as density functional theory(DFT) [28], inapplicable. We will, instead, exploit techniques based on many-body *Green's functions* which provide a unifying framework for the theoretical understanding of correlated electron systems. Even more important, these quantities are easily related to spectral functions which can be directly compared to corresponding experimental results from (one- or two-particle) spectroscopic measurements. In order to better highlight the physical aspect of these theoretical tools, we will reduce the formalities to a minimum. For a more complete discussion, we refer the reader to Ref. [29].

2.1. One-particle Green's function and the self-energy

The *one-particle* Green's function is defined as [30–32]

$$\begin{aligned} G(\nu, \mathbf{k}) &= \int_0^\beta d\tau\ e^{-i\nu\tau} G(\tau, \mathbf{k}) \\ &= \int_0^\beta d\tau\ e^{-i\nu\tau} \frac{1}{Z} \mathrm{Tr}[e^{-\beta\mathcal{H}} c^\dagger_{\mathbf{k}\sigma}(\tau) c_{\mathbf{k}\sigma}], \end{aligned} \tag{1}$$

where $\mathcal{H}$ denotes the Hamiltonian of the system and the operators $c^\dagger_{\mathbf{k}\sigma}$ ($c_{\mathbf{k}\sigma}$) create (annihilate) a particle with (lattice) momentum $\mathbf{k}$ and spin σ. $Z = \mathrm{Tr}[e^{-\beta\mathcal{H}}]$ (partition function) is a normalization factor and $\beta = 1/T$ the inverse of the temperature. The time evolution of the operator $c^\dagger_{\mathbf{k}\sigma}$ is given by $c^\dagger_{\mathbf{k}\sigma}(\tau) = e^{\tau\mathcal{H}} c^\dagger_{\mathbf{k}\sigma} e^{-\tau\mathcal{H}}$. Note that, for convenience, at finite temperature we adopt the Matsubara formalism, i.e., τ refers to an imaginary time and $i\nu = i(2n+1)\pi/\beta$ ($n \in \mathbb{Z}$) to a (fermionic) imaginary frequency. Moreover, we consider only the SU(2) symmetric case where the one-particle Green's function is spin-independent, i.e., $G_{\uparrow\uparrow}(\nu, \mathbf{k}) = G_{\downarrow\downarrow}(\nu, \mathbf{k}) \equiv G(\nu, \mathbf{k})$ and $G_{\uparrow\downarrow}(\nu, \mathbf{k}) = G_{\downarrow\uparrow}(\nu, \mathbf{k}) \equiv 0$.

From a physical perspective, $G(\tau, \mathbf{k})$ describes the amplitude for an excitation ("creation") of a hole or an electron [cf. operators $c_{\mathbf{k}\sigma}$ and $c^\dagger_{\mathbf{k}\sigma}$ in Eq. (1)] which propagates through the system for a (imaginary) time period τ until it is annihilated. During this propagation, which is described by the evolution operator $e^{-\tau\mathcal{H}}$, it scatters at other electrons in the system and, hence, $G(\tau, \mathbf{k})$ represents a measure of these scattering events (for a schematic illustration see upper panel of Fig. 2). After a Fourier transform to (imaginary) frequencies, these scattering event are even experimentally accessible. In fact, the imaginary part of $G(\omega, \mathbf{k})$ (obtained by an analytic continuation from imaginary frequencies ν to real frequencies ω) is related to the so-called spectral function $A(\omega, \mathbf{k}) = -\mathrm{Im}G(\omega, \mathbf{k})/\pi$ which can be measured,[1] e.g., by angular resolved photoemission spectroscopy (ARPES) experiments [2,39].

From a theoretical point of view, it is convenient to separate the scattering processes Σ of the excited particle (electron/hole) from its free propagation through the solid which we denote by G_0. The total amplitude G is then given by repeated alternating sequences of free propagation and scattering events which can be formally written as $G = G_0 + G_0\Sigma G_0 + G_0\Sigma G_0\Sigma G_0 + \cdots$. This has the form of a geometric series which can be summed, yielding the so-called Dyson equation

$$G(\nu, \mathbf{k}) = \frac{1}{G_0^{-1}(\nu, \mathbf{k}) - \Sigma(\nu, \mathbf{k})}, \tag{2}$$

where for a single-band system $G_0^{-1}(\nu, \mathbf{k}) = i\nu - \varepsilon_{\mathbf{k}}$ and $\varepsilon_{\mathbf{k}}$ is the dispersion relation of non-interacting electrons. The latter can be determined from the crystal structure of the lattice by means of DFT

[1] Here, we consider the sudden approximation for the theoretical description of photoemission process where so-called extrinsic losses due to scattering of the electron after its excitation on its way to the surface are neglected. This is justified for high enough energies of the incident photon and considers the "intrinsic" losses due to correlation effects which is assumed to be the most interesting part of the photoemission process for correlated systems. For a more comprehensive discussion of this question see Refs. [33–38,1].

calculations. *All* one-particle correlation effects on the other hand are described by the self-energy $\Sigma(\nu, \mathbf{k})$ which, hence, represents one of the central quantities in the theory of correlated many-electron systems.

2.2. Two-particle Green's function and the vertex

Similar to the one-particle Green's function in Eq. (1), one can define the two-particle Green's function as [29]:

$$G^{(2)}_{\sigma\sigma'}(k, k', q) = \int_0^\beta d\tau_1 d\tau_2 d\tau_3 \; e^{-i\nu\tau_1} e^{i(\nu+\Omega)\tau_2} e^{-i(\nu'+\Omega)\tau_3} \times \frac{1}{Z} \mathrm{Tr}[c^\dagger_{\mathbf{k}\sigma}(\tau_1) c_{(\mathbf{k}+\mathbf{q})\sigma}(\tau_2) c^\dagger_{(\mathbf{k}'+\mathbf{q})\sigma'}(\tau_3) c_{\mathbf{k}'\sigma}] \tag{3}$$

where ν and ν' are fermionic and Ω bosonic Matsubara frequencies, respectively [for the other definitions see Eq. (1)]. Here and in the following, we use the shorthand notation $k \triangleq (\nu, \mathbf{k})$ and $q \triangleq (\Omega, \mathbf{q})$ of combined frequency/momentum variables (four-vector) whenever it is convenient. Analogously to $G(k)$ in Eq. (1), $G^{(2)}_{\sigma\sigma'}(k, k', q)$ describes the excitation of *two* particles/holes (or one particle and one whole) and their propagation through the system. From a more practical perspective, $G^{(2)}_{\sigma\sigma'}(k, k', q)$ contains a wealth of experimentally accessible information. For instance, by summing/integrating this quantity over k and k' one obtains physical *response functions* (susceptibilities) $\chi_r(\Omega, \mathbf{q})$:

$$\chi_{\mathrm{ch}}(i\Omega, \mathbf{q}) = \sum_{\mathrm{kk'}} G^{(2)}_{\uparrow\uparrow}(k, k', q) + G^{(2)}_{\uparrow\downarrow}(k, k', q) - \beta\frac{n^2}{4}\delta_{q0}, \tag{4a}$$

$$\chi_{\mathrm{sp}}(i\Omega, \mathbf{q}) = \sum_{\mathrm{kk'}} G^{(2)}_{\uparrow\uparrow}(k, k', q) - G^{(2)}_{\uparrow\downarrow}(k, k', q), \tag{4b}$$

$$\chi_{\mathrm{pp}}(i\Omega, \mathbf{q}) = \sum_{\mathrm{kk'}} G^{(2)}_{\uparrow\downarrow}(k, k', q - k - k'), \tag{4c}$$

where $\sum_k \triangleq \frac{1}{\beta}\sum_\nu \frac{1}{V_{\mathrm{BZ}}}\int_{\mathrm{BZ}} d^dk$ denotes the (Matsubara) frequency summation and momentum integration over the d-dimensional Brillouin with the volume V_{BZ}. The labels r = ch(arge), sp(in) and pp (particle–particle) refer to the response of the system to a change in the chemical potential, an external magnetic field and a pairing field, respectively.[2] Multiplying $G^{(2)}_{\mathrm{ch}}(k, k', q) = G^{(2)}_{\uparrow\uparrow}(k, k', q) + G^{(2)}_{\uparrow\downarrow}(k, k', q)$ in Eq. (4a) with the electromagnetic current operators [41] $\mathbf{v}_i(\mathbf{k}) = d\varepsilon_{\mathbf{k}}/dk_i$ and $\mathbf{v}_j(\mathbf{k}')$ before the summation over k and k' yields the linear response of the system to an external electromagnetic field, i.e., the optical conductivity $\sigma_{ij}(\omega)$ (for $i\Omega \to \omega + i\delta$ and the limit of long wave lengths $\mathbf{q} = 0$). Let us point out that all these physical response functions are in some sense "reduced" two-particle correlation functions as two of the three frequencies (as well as the corresponding momenta) which appear in the definition of $G^{(2)}$ in Eq. (3) are summed (integrated) over. The question, whether two-particle coincidence spectroscopy will allow for a more complete comparison with $G^{(2)}$ is touched in Section 4.

Let us now analyze the structure of the two-particle Green's function in Eq. (3). For noninteracting electrons, $G^{(2)}_{\sigma\sigma'}(k, k'q)$ corresponds to the independent propagation of two particles/holes (or one particle and one hole) which is represented by products of one-particle Green's functions, i.e., $G^{(2)}_{\sigma\sigma'}(k, k'q) = G(k)G(k')\delta_{q0} - G(k)G(k+q)\delta_{\mathrm{kk'}}\delta_{\sigma\sigma'}$. In the presence of interactions between the particles, an additional term arises which describes the correlations between the two excited electrons or holes. Similarly as in the one-particle situation, it is advantageous to separate this correlated part from the full two-particle correlation function $G^{(2)}_{\sigma\sigma'}(k, k'q)$. Formally, this is achieved by the definition of the so-called vertex function $F^{\mathrm{kk'}q}_{\sigma\sigma'}$ which is defined as

$$F^{\mathrm{kk'}q}_{\sigma\sigma'} = -\frac{G^{(2)}_{\sigma\sigma'}(k, k', q) - G(k)G(k')\delta_{q0} + G(k)G(k+q)\delta_{\mathrm{kk'}}\delta_{\sigma\sigma'}}{G(k)G(k+q)G(k'+q)G(k')}, \tag{5}$$

where in the numerator the above discussed noninteracting part of $G^{(2)}$ is subtracted and the one-particle Green's function in the denominator remove the independent propagation of the particles before and after the scattering process. Physically, $F^{\mathrm{kk'}q}_{\sigma\sigma'}$ corresponds to the full scattering amplitude between two particles or holes [30] within our many-electron system (for a graphical illustration see lower panel of Fig. 2). From a different perspective, this can be also interpreted as scattering of a single particle at a collective mode (e.g., charge, spin or superconductivity) which will be discussed in Section 3.1. Moreover, $F^{\mathrm{kk'}q}_{\sigma\sigma'}$ can be decomposed into different scattering channels which will be considered in Section 3.2.

2.3. Relating one- and two-particle scattering amplitudes: the equation of motion (EOM)

In the two previous sections, we have discussed the one- and the two-particle scattering amplitudes $\Sigma(k)$ and $F^{\mathrm{kk'}q}_{\sigma\sigma'}$, respectively, which describe correlation effects in a many electron system. On a microscopic level, such correlations are typically generated by a two-body Coulomb interaction between the particles. Consequently, the one-particle scattering amplitude $\Sigma(k)$ must correspond to the sum of all two-particle scattering events which an electron experiences when it propagates through the system (see Fig. 2). This implies that there must be a connection between $\Sigma(k)$ and $F^{\mathrm{kk'}q}_{\sigma\sigma'}$. Such a relation, which can be obtained from a time derivative of $G(\tau, \mathbf{k})$, is provided by the EOM. For the case of a purely local interaction U between ↑- and ↓-electrons (Hubbard model) [4] it takes the form

$$\Sigma(k) = \frac{\mathrm{Un}}{2} - \frac{U}{\beta^2}\sum_{k'q} F^{\mathrm{kk'}q}_{\uparrow\downarrow} G(k')G(k'+q)G(k+q), \tag{6}$$

where n denotes the average number of particles per lattice site and $G(k)$ is the fully renormalized one-particle Green's function given in Eq. (2). The interpretation of this equation, which is illustrated graphically in Fig. 3 in terms of Feynman diagrams, is straightforward: As anticipated, the total one-particle scattering amplitude $\Sigma(k)$ is the average over all two-particle scattering events $F^{\mathrm{kk'}q}_{\sigma\sigma'}$. This insight will guide our way to develop various approaches for analyzing the self-energy $\Sigma(k)$ in terms of the two-particle vertex $F^{\mathrm{kk'}q}_{\sigma\sigma'}$ which will be discussed in Section 3.

It should be mentioned that there is another constraint which connects one- and two-particle correlations functions. This follows from the symmetries and the related conservation laws of the system and can be expressed in its differential form as the *Ward identity* $\frac{\delta\Sigma[G]}{\delta G} = F_{\mathrm{irr}}$ where F_{irr} is the so-called *irreducible* part of the full vertex [42,43] F (for more details see, e.g., Ref. [29]). In an exact treatment, *both* the Ward identity and the EOM (6) are fulfilled. For approximate theories, however, often at least one of these relations is violated.[3] Hence, when choosing a certain approximation for the calculation of Σ and F one has to decide which of the two connections between Σ and $F_{(\mathrm{irr})}$ is more important for the intended application. The methods which will be discussed in the following are all based on the EOM (6) and consequently it is necessary that the selected approach for calculating Σ and F respects this relation. On the other hand, one has to keep in mind that this can in general lead to violations of Ward identities and the related conservation laws.

[2] For $i\Omega \equiv 0$ one obtains the *isothermal* response, i.e., the system remains connected to a thermal bath after the external perturbation. The analytic continuation $i\Omega \to \omega + i\delta$, on the other hand, gives rise to the so-called Kubo-response where the system is isolated after the external perturbation [40].

[3] For approximations based on Feynman diagrammatic expansions of Σ and $F_{(\mathrm{irr})}$ it can be even shown [44–46] that Ward identities and the EOM cannot be fulfilled simultaneously unless *all* diagrams are taken into account (corresponding to the exact solution of the problem).

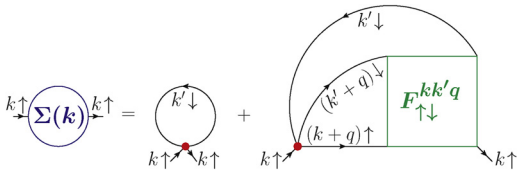

Fig. 3. Feynman diagrammatic representation of the EOM. Solid black lines denote full (interacting) one-particle Green's functions $G(k)$ [Eq. (2)] and red dots correspond to the bare Hubbard interaction U. The four vector notation $k \triangleq (\nu, \mathbf{k})$ and $q \triangleq (\Omega, \mathbf{q})$ has been adopted. The first term on the right hand side corresponds to the Hartree contribution $\frac{\mathrm{Un}}{2}$.

3. Dissecting the spectral function – the pseudogap in the cuprates

In this section, we want to clarify the origin of the pseudogap in the cuprates (see Fig. 1) by exploiting Eq. (6). Our general strategy to achieve this is the following: (i) In the first step, we construct a model Hamiltonian which captures the relevant physics which we want to describe, i.e., whose $\Sigma(k)$ contains (at least qualitatively) the spectral features which are experimentally observed. (ii) Secondly, we choose a method to calculate the one- and two-particle Green's functions of our system. In this connection, it is very important that $\Sigma(k)$ and $F^{\mathrm{kk'}q}_{\sigma\sigma'}$ are computed on equal footing and that the vertex is obtained in an unbiased way.[4] (iii) In the final step, we examine which contributions of $F^{\mathrm{kk'}q}_{\sigma\sigma'}$ in Eq. (6) are responsible for certain features in $\Sigma(k)$. In practice, this can be achieved in different ways, three of which we will discuss in this paper. In Section 3.1 we analyze for which values of q the contribution of $F^{\mathrm{kk'}q}_{\sigma\sigma'}$ is largest [24] ("Fluctuation Diagnostics"). In Section 3.2, we exploit a diagrammatic decomposition of the vertex $F^{\mathrm{kk'}q}_{\sigma\sigma'}$ into various scattering channels and investigate their different contributions to $\Sigma(k)$ [25]. Finally, in Section 3.3 we identify the many-particle state (s) which yield the most relevant contributions to $F^{\mathrm{kk'}q}_{\sigma\sigma'}$ and are, hence, responsible for the emergence of specific features in the self-energy [26] (such as the pseudogap).

Let us note that the above described procedures can be used for two different purposes. Apart from identifying the relevant two-particle processes which are responsible for the physics of the system, they can also determine the quality of the theoretical model which is used for the description of experimental findings. In fact, if our analysis disagrees with other experimental results for two-particle correlation functions [e.g., the susceptibilities in Eq. (4)], we can conclude that our modelization needs to be improved.

Let us also stress, that the analysis of $\Sigma(k)$ in terms of $F^{\mathrm{kk'}q}_{\sigma\sigma'}$ is obviously not restricted to the case of the pseudogap in the cuprates which is considered here, but is applicable more generally for the analysis of spectra of correlated systems whenever experimental and/or theoretical techniques allow for an accurate and unbiased determination of the two-particle scattering amplitude.

Model and method. The minimal model for the description of the pseudogap physics in the cuprates is the single-band Hubbard model on a two-dimensional ($2d$) square lattice

$$\mathcal{H} = -t \sum_{\langle \mathrm{ij}\rangle,\sigma} c^{\dagger}_{i\sigma} c_{j\sigma} - t' \sum_{\langle\langle \mathrm{ij}\rangle\rangle,\sigma} c^{\dagger}_{i\sigma} c_{j\sigma} + U \sum_{i} n_{i\uparrow} n_{i\downarrow}, \tag{7}$$

where t and t' denote the hopping amplitudes for the electrons between nearest and next-nearest neighbors i and j, respectively, $n_{i\sigma} = c^{\dagger}_{i\sigma} c_{i\sigma}$, and U is the potential energy for two electrons occupying the same site. Let us remark that, although this model has been often assumed to describe the essential physics of the cuprates, it has been recently argued that a multi-orbital extensions (e.g., a three-orbital Emery model) is required [47] for an adequate theoretical treatment.

In order to calculate $\Sigma(k)$ and $F^{\mathrm{kk'}q}_{\sigma\sigma'}$ for the Hubbard model in Eq. (7), we will adopt the dynamical cluster approximation [48] (DCA) with N_c nonequivalent k-points in the Brillouin zone. This approach approximates the lattice of interacting sites by a small cluster in momentum space which is self-consistently embedded into a dynamic bath. In this way, all local and nonlocal correlation effects within the cluster size are captured exactly while long-range correlations are treated on a mean-field level. For the case of $N_c = 1$, DCA becomes equivalent to the dynamical mean-field theory [49] (DMFT) which has been successfully exploited to describe physical properties of realistic correlated materials [50,51]. DCA allows to compute $\Sigma(k)$ and $F^{\mathrm{kk'}q}_{\sigma\sigma'}$ in an *unbiased* way without any *a priori* assumptions about the physics of the system and is, hence, suited as basis for the diagnostic methods which will be outlined in the following sections.

3.1. Choosing the best perspective – "Fluctuation Diagnostics"

Eq. (6) allows us to calculate the self-energy through summing/integrating the vertex $F^{\mathrm{kk'}q}_{\uparrow\downarrow}$ (multiplied by three Green's function) over the frequencies/momenta $k' = (\nu', \mathbf{k'})$ and $q = (\Omega, \mathbf{q})$, respectively. It is then very natural to ask which contributions of this sums/integrals are the most relevant ones for the emergence of specific features in $\Sigma(k)$. This question is at the heart of the so-called "Fluctuation Diagnostics" approach which has been put forward in Ref. [24]. Its basic idea is to perform *partial* summations in Eq. (6) which allows us to "dissect" the total self-energy into contributions originating from different frequencies and/or momenta. More specifically, for the "Fluctuation Diagnostics" one carries out the summation/integration over the fermionic frequency/momentum $k' = (\nu', \mathbf{k'})$ and analyses the contributions to $\Sigma(k)$ which originate from different values of $q = (\Omega, \mathbf{k})$. In practice, this is achieved by considering the two functions

$$\tilde{\Sigma}_{\mathbf{q}}(k) = -\frac{U}{\beta^2} \sum_{k'\Omega} F^{\mathrm{kk'}q}_{\uparrow\downarrow} G(k') G(k'+q) G(k+q), \tag{8a}$$

$$\tilde{\Sigma}_{\Omega}(k) = -\frac{U}{\beta^2} \sum_{k'\mathbf{q}} F^{\mathrm{kk'}q}_{\uparrow\downarrow} G(k') G(k'+q) G(k+q), \tag{8b}$$

which correspond to the EOM (6) apart from leaving out the integration/summation over $\mathbf{q}$ and Ω, respectively. The full self-energy $\Sigma(k)$ can be obviously reproduced by integrating/summing these functions over $\mathbf{q}$ or Ω

$$\Sigma(k) - \frac{\mathrm{Un}}{2} = \sum_{\mathbf{q}} \tilde{\Sigma}_{\mathbf{q}}(k) = \sum_{\Omega} \tilde{\Sigma}_{\Omega}(k). \tag{9}$$

Unfortunately, a straightforward interpretation of the dissection of the self-energy in the form of Eq. (8a) or (8b) is not yet possible since the $\uparrow\downarrow$ vertex which enters these relations cannot be directly associated to physical (charge, spin or particle–particle) fluctuations. To overcome this problem, we exploit the possibility to express the EOM in different representations. In fact, in the SU(2) symmetric case $F^{\mathrm{kk'}q}_{\uparrow\downarrow}$ can be replaced in Eq. (6) by the corresponding charge ($F^{\mathrm{kk'}q}_{\mathrm{ch}} = F^{\mathrm{kk'}q}_{\uparrow\uparrow} + F^{\mathrm{kk'}q}_{\uparrow\downarrow}$), (negative) spin ($-F^{\mathrm{kk'}q}_{\mathrm{sp}} = -F^{\mathrm{kk'}q}_{\uparrow\uparrow} + F^{\mathrm{kk'}q}_{\uparrow\downarrow}$), or particle–particle[5] ($F^{\mathrm{kk'}q}_{\mathrm{pp}} = F^{\mathrm{kk'}(q-k-k')}_{\uparrow\downarrow}$) vertex. If all summations/integrations over k' and q are performed in Eq. (6) we obtain the same result for $\Sigma(k)$ independent of the representation of the vertex. On the contrary, the partially summed quantities $\tilde{\Sigma}_{\mathbf{q}}(k)$ and $\tilde{\Sigma}_{\Omega}(k)$ will strongly depend on the choice of the representation which provides crucial information about the impact of certain fluctuations on the self-energy. If, for a given representation (channel) r = ch, sp or pp, $\tilde{\Sigma}_{\mathbf{q}}(k)$ is strongly peaked at a

[4] If $F^{\mathrm{kk'}q}_{\sigma\sigma'}$ is obtained within an approximation which favors certain types of two-particle scattering events or specific collective modes, the diagnostics of the self-energy via Eq. (6) will obviously come to the conclusion that these *a priori* introduced physical processes are responsible for the features observed in $\Sigma(k)$.

[5] For this replacement, also the arguments of the Green's functions inside the sum/integral on the right hand side of Eq. (6) have to be modified according to $q \to q - k - k'$.

specific transferred momentum $\mathbf{q} = \mathbf{q_0}$ and small for all other momenta, $\Sigma(k)$ is mainly determined by strong long-range fluctuations in this channel. The vector $\mathbf{q_0}$ defines the spatial structure of this collective mode via the Fourier factor $e^{i\mathbf{q_0}\mathbf{R}_i}$ (where $\mathbf{R}_i$ is a lattice vector). For instance, in the spin representation a strong peak of $\tilde{\Sigma}_{\mathbf{q}}(k)$ at $\mathbf{q_0} = (\pi, \pi)$ signals that $\Sigma(k)$ is mainly governed by antiferromagnetic spin fluctuations while $\mathbf{q_0} = (0, 0)$ indicates the dominance of a ferromagnetic mode. In the charge picture, an enhanced $\tilde{\Sigma}_{\mathbf{q}}(k)$ for $\mathbf{q_0} = (\pi, \pi)$ marks the dominant role of charge density wave (CDW) fluctuations while a peak at $\mathbf{q_0} = (0, 0)$ in the particle–particle representation reveals the importance of long-range *s*-wave pairing fluctuations. On the other hand, if for a given channel $\tilde{\Sigma}_{\mathbf{q}}(k)$ is almost independent of $\mathbf{q}$ the corresponding fluctuations are short ranged and, hence, do not represent a collective bosonic mode of the electrons in the system. An analogous analysis can be performed for $\tilde{\Sigma}_{\Omega}(k)$ where a strong peak at $\Omega = 0$ indicates stable *long-lived* fluctuations in the corresponding channel while a (almost) Ω-independent behavior signals that fluctuations in this channel are relevant only on very short time scales. In this respect, it would be very interesting to conduct this type of analysis also in the (real) time domain. This, however, would require an analytic continuation of the vertex $F^{\mathbf{k}\mathbf{k}'q}_{\uparrow\downarrow}$ from imaginary (ν, ν' and Ω) to real (ω_1, ω_2 and ω_3) frequencies and a subsequent Fourier transform to real times (t_1, t_2 and t_3). At present, such an analytical continuation for vertex functions is *not* available which prevents a direct application of our method in the *real* frequency/time domain.

Let us stress, that each system can be of course described in each of the channels r = ch, sp and pp. However, the most suitable representation is the one for which $\tilde{\Sigma}_{\mathbf{q}}(k)$ and $\tilde{\Sigma}_{\Omega}(k)$ exhibit a strongly peaked behavior in $\mathbf{q}$ and Ω, respectively, as this is a clear hallmark of the dominant role of long-living and long-ranged fluctuations in this channel (i.e., a collective bosonic mode) which is then responsible for the features in $\Sigma(k)$. This situation can be compared to the dynamics of the planets in our solar system: In principle, all coordinate systems are equivalent for the description of this problem, but as we know, the heliocentric reference system is definitely more suitable for the physical understanding than its geocentric counterpart.

Results for the Hubbard model. We have applied the "Fluctuation Diagnostics" method to the Hubbard Hamiltonian [Eq. (6)] for a set of parameters which are relevant for the pseudogap regime of the cuprates (for the exact values see the caption of Fig. 4). Our model reproduces well the experimentally observed pseudogap feature as one can see from the insets in Fig. 4: For the nodal point $\mathbf{k} = (0, \pi)$ (left) one observes a large value of $\Sigma(k)$ at the lowest Matsubara frequency $\nu = \pi/\beta$ which corresponds to a suppression of spectral weight in $A(\omega, \mathbf{k})$ while the antinodal point $\mathbf{k} = (\pi/2, \pi/2)$ exhibits a metallic behavior for the self-energy which is reflected by a peak in the spectral function at $\omega = 0$. The lower panels depict the functions $\tilde{\Sigma}_{\mathbf{q}}(k)$ at the lowest Matsubara frequency ($\nu = \pi/\beta$) and the two selected $\mathbf{k}$-points for the eight $\mathbf{q}$ vectors in the DCA cluster in all three channels r = ch, sp and pp. In the charge- and the particle–particle representation one observes a uniform $\mathbf{q}$ distribution for both $\mathbf{k}$-values which prevents an interpretation of the pseudogap phenomenon in terms of charge or *s*-wave pairing fluctuations. On the contrary, the corresponding results for the spin-channel are strongly peaked at $\mathbf{q} = (\pi, \pi)$. According to the discussion above, this indicates that long-range antiferromagnetic spin fluctuations are responsible for the large value of $\Sigma(k)$ at the lowest Matsubara frequency. Moreover, also the strong momentum differentiation between $\mathbf{k} = (0, \pi)$ and $\mathbf{k} = (\pi/2, \pi/2)$ follows from the different sizes of $\tilde{\Sigma}_{\mathbf{q}=(\pi,\pi)}(k)$ for the antinodal and nodal $\mathbf{k}$ point, respectively. Hence, we conclude that long range antiferromagnetic spin fluctuations are responsible for the pseudogap behavior of $\Sigma(k)$ in the Hubbard model. A corresponding analysis of $\tilde{\Sigma}_{\Omega}(k)$ indeed confirms [24] that this fluctuations are long-living and, therefore, represent a well defined mode.

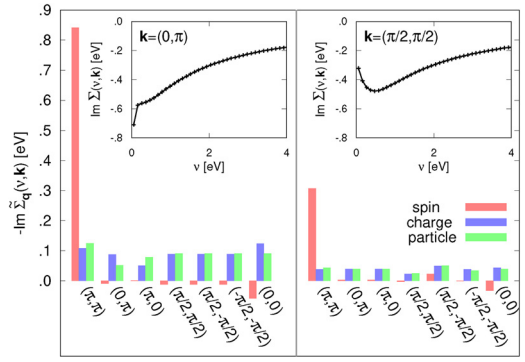

Fig. 4. "Fluctuation Diagnostics" of the DCA self-energy $\Sigma(k)$ for $N_c = 8$, $t = -0.25$ eV, $t' = 0.0375$ eV, $U = 1.75$ eV, $n = 0.94$ and $\beta = 60\,\text{eV}^{-1}$. The insets show the frequency dependence of the self-energy $\Sigma(k)$ for the two (cluster) momenta $\mathbf{k} = (0, \pi)$ and $\mathbf{k} = (\pi/2, \pi/2)$ on the Fermi surface, respectively. The main panel depicts the contribution to $\Sigma(k)$ for the first Matsubara frequency $\nu = \pi/\beta$ from the different transferred momenta $\mathbf{q}$ in the three representations of the vertex (spin, charge, particle–particle). The figure has been readapted from Ref. [24].

3.2. Disassembling the vertex – parquet decomposition of the self-energy

A dissection of the self-energy via Eq. (6) can be also achieved by disentangling the different two-particle scattering processes which contribute to the full vertex $F^{\mathbf{k}\mathbf{k}'q}_{\uparrow\downarrow}$. The representation of $F^{\mathbf{k}\mathbf{k}'q}_{\uparrow\downarrow}$ in terms of Feynman diagrams provides a natural framework for this objective. Each Feynman diagram describes a specific two-particle scattering process and the full vertex corresponds to the sum of all such diagrams. One can then divide this set of all diagrams into different groups according to the physical mechanisms which they describe. Such a decomposition is provided by the parquet formalism [52,45,29] which allows us to split the full two-particle scattering amplitude $F^{\mathbf{k}\mathbf{k}'q}_{\uparrow\downarrow}$ into *four* distinct classes which are defined by the topological structure of the Feynman diagrams which they contain, i.e., by the different ways in which a diagram can be decomposed into two-parts by cutting two internal propagators (see dashed lines in Fig. 5). For a more rigorous derivation of this concept we refer the reader to the literature [45,29,53]. Here, instead we want to avoid most of the technical details and give a more physical explanation of the four different parts into which $F^{\mathbf{k}\mathbf{k}'q}_{\sigma\sigma'}$ can be separated as it is depicted in Fig. 5. The first contribution is the fully irreducible vertex Λ which contains the "direct" interaction between the two electrons and consists of diagrams which cannot be split by cutting two internal lines (in its lowest order it is given by the bare U). The three other classes Φ_r contain reducible diagrams in one of the three channels r = ch, sp or pp which can be separated into two parts by cutting two internal lines. These are also called ladder diagrams which describe a repeated scattering of the particles in the given channel and, hence, account for the effect collective fluctuations. In fact, these functions will get very large in regions where the corresponding fluctuations increase which is indicated by a simultaneous increase of the physical susceptibilities in Eq. (4).

We can now insert the decomposition of $F^{\mathbf{k}\mathbf{k}'q}_{\uparrow\downarrow}$ as given in the first line of Fig. 5 into the EOM (6) which naturally leads to a corresponding separation of $\Sigma(k)$ into four parts:

$$\Sigma(k) = \tilde{\Sigma}_{\Lambda}(k) + \tilde{\Sigma}_{\text{pp}}(k) + \tilde{\Sigma}_{\text{ch}}(k) + \tilde{\Sigma}_{\text{sp}}(k), \tag{10}$$

where the single contributions are obtained by replacing $F^{\mathbf{k}\mathbf{k}'q}_{\uparrow\downarrow}$ in Eq. (6) by $\Lambda^{\mathbf{k}\mathbf{k}'q}_{\uparrow\downarrow}$ and $\Phi^{\mathbf{k}\mathbf{k}'q}_{r,\uparrow\downarrow}$, respectively.

Results for the Hubbard model. We have applied the decomposition in Eq. (10) to the DCA solution of the 2*d* Hubbard model for the same parameters as in Section 3.1 (see caption of Fig. 4) with the only minor difference that we have considered $t' = 0$ which does not qualitatively change the properties of the system [see $\Sigma(k)$ (black curves) in Fig. 6]. The results of the decomposition are shown in the insets of the upper and the lower panel of Fig. 6 for the antinodal and the nodal point on the Fermi surface. Unfortunately, the various contributions show a

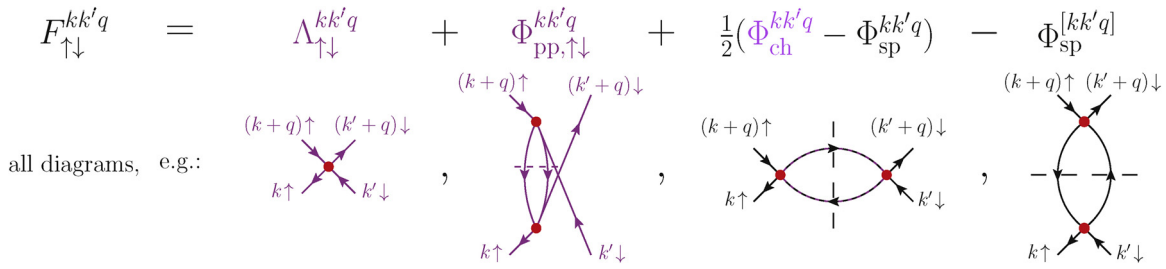

Fig. 5. Diagrammatic representation of the parquet decomposition (let us stress that the label "parquet decomposition" refers here only to a separation of diagrams into the different scattering channels rather than to a self-consistent solution [54–56] of the parquet equations) of the full two-particle scattering amplitude $F^{kk'q}_{\uparrow\downarrow}$. Solid lines denote fully renormalized Green's functions $G(\nu, \mathbf{k})$ form Eq. (2) [corresponding to a so-called skeleton diagrammatic expansion [29]] and red dots represent the bare Hubbard interaction U. The brackets ("[]") in the argument of the rightmost contribution indicate that the frequency arguments of this vertex are k, $k + q$ and $k' - k$ rather than k, k' and q which, however, is not relevant when the vertex is used in the EOM.

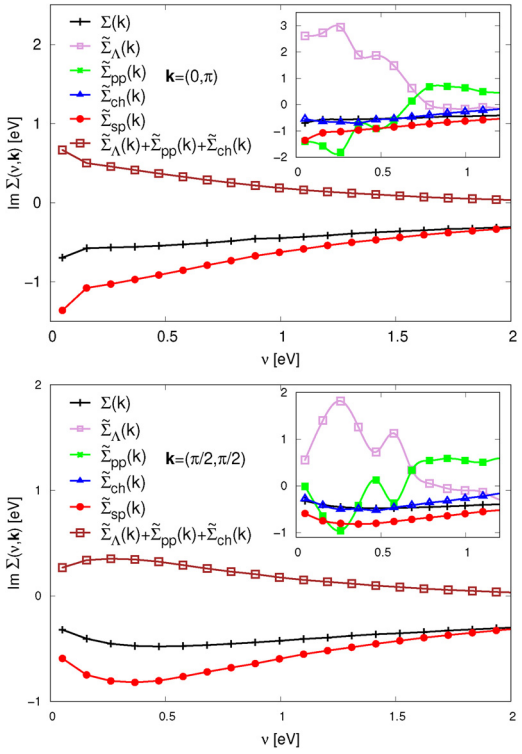

Fig. 6. Parquet decomposition of the DCA self-energy of the 2*d* Hubbard model for the same parameters as in Fig. 4 with the only difference that here $t' = 0$. The figure has been readapted from Ref.[25].

highly fluctuating behavior with maxima and minima essentially larger than the self-energy itself which prevents a straightforward physical interpretation.[6] One can trace this unexpected result back to the emergence of low-energy singularities in Λ and Φ_r which are observed already in the intermediate coupling regime, even before the onset of the Mott metal-to-insulator transition [57–59,25,60,61,26,62,63]. This restricts the applicability of the parquet decomposition for the self-energy to the weak-coupling regime where it indeed yields reasonable results [25].

By a closer inspection of the insets of Fig. 6 one observes that one contribution is not affected by fluctuations, i.e., $\tilde{\Sigma}_{sp}(k)$. This suggests a separation of the total self-energy into its spin-part and a "rest" function which corresponds to the sum of all other contributions (Λ, Φ_{ch} and $\Phi_{pp,\uparrow\downarrow}$, violet diagrams in Fig. 5). The results of this analysis are reported in the main panels of Fig. 6. One can clearly see that the large values of the self-energy (black) originate from the spin contribution $\tilde{\Sigma}_{sp}(k)$ (red) which describes scattering processes in the spin channel. $\tilde{\Sigma}_{sp}(k)$ is also responsible for the large momentum differentiation between $\mathbf{k} = (0, \pi)$ (upper panel) and $\mathbf{k} = (\pi/2, \pi/2)$ (lower panel) which confirms the results from the "Fluctuation Diagnostics" in Section 3.1. Notably, $\tilde{\Sigma}_{sp}(k)$ even overestimates the self-energy. This is compensated by the contributions of the other scattering channels (brown) which, hence, provide a screening of the dominant spin fluctuations.

3.3. Spectral functions and ground states

The methods presented in Sections 3.1 and 3.2 allow us to identify the type of collective bosonic fluctuations which generate certain features in the electronic self-energy and the spectral function of a system. However, they do not provide any insights about the underlying quantum mechanical many-body ground state which is responsible for this type of physics. Such information can be also extracted from Eq. (6) through a slight modification of the ideas which have been introduced in the "Fluctuation Diagnostics" method. By multiplying Eq. (6) with $G(k)$ and performing the summations/integrations over q and ν' we obtain a function $B_{\mathbf{k}'}(k)$ which describes the contributions to $\Sigma(k)$ originating from different fermionic momenta $\mathbf{k}'$. Considering Eqs. (3) and (5) for very low temperatures and very large interactions (i.e., $\nu = \pi/\beta \lll U$) we can express $B_{\mathbf{k}'}(k)$ approximately as

$$B_{\mathbf{k}'}(k) = -2\langle n_{\mathbf{k}'}\rangle - 4\sum_{\mathbf{R_1R_2}} e^{i(\mathbf{k}-\mathbf{k}')(\mathbf{R_1}-\mathbf{R_2})} \times \langle E_0(N)|c^\dagger_{\mathbf{R_2}\downarrow}c_{\mathbf{R_2}\uparrow}c^\dagger_{\mathbf{R_1}\uparrow}c_{\mathbf{R_1}\downarrow}|E_0(N)\rangle, \quad (11)$$

where $\mathbf{R_i}$ are lattice vectors and $|E_0(N)\rangle$ denotes the ground state of the system with N particles and a ground state energy $E_0(N)$ (for a detailed description of all approximations which have been exploited to derive Eq. (11) we refer the reader to Ref. [26]). Summing $B_{\mathbf{k}'}(k)$ over $\mathbf{k}'$ yields $\Sigma(k)G(k)$. For the situation of the Hubbard model which has been discussed in the two previous sections we obtain [26] that $B_{\mathbf{k}'}(k)$ yields a large (negative) contribution for $\mathbf{k}' = \mathbf{k} + (\pi, \pi)$. Considering the SU(2) symmetry, this corresponds exactly to the strong peak in $\tilde{\Sigma}_{\mathbf{q}}(k)$ in the spin representation for the transferred momentum $\mathbf{q} = (\pi, \pi)$ and, hence, indicates the dominant role of antiferromagnetic fluctuations for the emergence of the pseudogap. It can be then shown that a large value of $B_{\mathbf{k}'}(k)$ for $\mathbf{k}' = \mathbf{k} + (\pi, \pi)$ is obtained for a ground state $|E_0(N)\rangle$ which is built from spin-singlets of the form

$$|(12)\rangle = \frac{1}{\sqrt{2}}(c^\dagger_{\mathbf{R_1}\uparrow}c^\dagger_{\mathbf{R_1}\downarrow} - c^\dagger_{\mathbf{R_1}\downarrow}c^\dagger_{\mathbf{R_1}\uparrow}). \quad (12)$$

This state represents valence bonds between neighboring lattice sites $\mathbf{R_1}$ and $\mathbf{R_2}$ and the full resonating valence bond (RVB) ground state [64] can be constructed as a superposition of all possible valence bond states between all sites of the lattice.

We can now sum up our analysis of the pseudogap physics as

[6] Note that we have carefully checked that the sum of all these strongly fluctuating contributions indeed reproduces the exact DCA self-energy of the system.

follows: A large value of $\Sigma(k)$ originates from long ranged antiferromagnetic fluctuations represented by a large value of $B_{\mathbf{k}'}(k)$ for $\mathbf{k}' = \mathbf{k} + (\pi, \pi)$. The latter, in turn, is mainly due to the formation of a RVB ground state which allows to relate the pseudogap feature in the self-energy to the emergence of a RVB state in the lattice.

4. Summary and future perspectives: coincidence spectroscopy and vertex functions

In this work, we have reviewed different techniques for analyzing the electronic self-energy of a correlated electron system. The described approaches exploit an exact relation between $\Sigma(k)$ and the vertex $F^{kk'q}_{\uparrow\downarrow}$ which is coined EOM [Eq. (6)]. This equation expresses $\Sigma(k)$ as an average over $F^{kk'q}_{\uparrow\downarrow}$ which allows for an identification of the two-particle scattering processes which are most relevant for specific features in the self-energy. More specifically, we have presented three different ways how Eq. (6) can be used to "dissect" $\Sigma(k)$ and have applied them to resolve the origin of the pseudogap feature which emerges in the 2*d* Hubbard model in parameter regimes which are relevant for the description of the high-temperature superconducting cuprates.

In the "Fluctuation Diagnostics" approach (Section 3.1), we have performed partial summations in the EOM in different representations (charge, spin or particle–particle) in order to unravel the contributions originating from different transferred momenta $\mathbf{q}$ and transferred frequencies Ω. If for a given representation such a decomposition of $\Sigma(k)$ is strongly peaked at a given $\mathbf{q} = \mathbf{q}_0$ and $\Omega = 0$, respectively, the self-energy is mainly determined by long-ranged and long-lived fluctuations in this channel whose spatial structure is determined by the vector $\mathbf{q}_0$. On the contrary, for an "inappropriate" representation the separation of $\Sigma(k)$ into different $\mathbf{q}$ and Ω contributions will be rather uniform which prevents an interpretation in terms of well-defined collective bosonic mode. By means of the "Fluctuation Diagnostics", we have identified antiferromagnetic spin fluctuations as driving force for the emergence of the pseudogap feature in the 2*d* Hubbard model while charge and particle–particle fluctuations are only short-ranged and short-lived.

Instead of disentangling the frequency and momentum sums/integrations in Eq. (6), one can alternatively use the parquet formalism to disassemble the vertex $F^{kk'q}_{\uparrow\downarrow}$ into different scattering channels, as proposed in Section 3.2. While a full decomposition breaks down at intermediate-to-strong coupling due to singularities in the irreducible parts of the vertex, a splitting of $F^{kk'q}_{\uparrow\downarrow}$ into the dominant channel and a "rest" function containing all the other channels is always possible. For the 2*d* Hubbard model this approach has confirmed the picture of the "Fluctuation Diagnostics" and identified spin fluctuations as the major mechanism for the suppression of spectral weight at the Fermi level while the "rest" function represents as a screening for the dominant spin channel which would otherwise overestimate the size of the pseudogap.

Finally, in Section 3.3 we have exploited a decomposition of $\Sigma(k)$ into the fermionic frequencies and momenta ν' and $\mathbf{k}'$, respectively, in order to relate the appearance of a pseudogap, which is due to long-range antiferromagnetic fluctuations, to the formation of a RVB ground state in the system.[7] This demonstrates the possibility to extract even information about the importance of different quantum mechanical many-body states for the physics of the system from an analysis of the EOM.

From a purely theoretical perspective, the above described approaches can be applied to a large variety of model systems for which an unbiased evaluation of the two-particle vertex function $F^{kk'q}_{\uparrow\downarrow}$ is possible. In order to make these methods more directly applicable to experimental results, techniques for measuring two-particle correlation functions are highly desirable. However, most of the existing experiments determine only "reduced" two-particle correlation functions which depend only on *one* frequency and/or momentum, such as the optical conductivity or different types of susceptibilities [see, e.g., Eq. (4)].

Two-particle coincidence spectroscopy [65,66] might provide a versatile tool to experimentally map out two-particle correlations in correlated systems more comprehensively. The realization of such ideas certainly requires an improved theoretical understanding of this experimental technique. In fact, while a theoretical interpretation of one-particle spectroscopic experiments (e.g., ARPES) in terms of self-energies and spectral functions has become standard in the last decades [34–36,39], no comparable level of understanding for the two-particle coincidence spectroscopy has been achieved so far. For weakly interacting systems, the two-particle spectrum can be approximated to a good accuracy by a convolution of two single-particle spectra. Such an approach obviously breaks down in the presence of (strong) correlations where vertex corrections have to be considered. The paths which have been followed hitherto to tackle this problem were based on the Feshbach projection technique [67], nonequilibrium Green's functions [67] and DMFT [68]. While these approaches have produced first encouraging results for the description of two-particle coincidence spectra they are mainly based on reduced two-particle correlation functions which depend on only one rather than on three frequencies. Establishing a more direct relation between coincidence spectroscopy data and theoretically calculable vertex functions represents therefore a highly promising future research direction.

[7] Let us note that the analysis of Section 3.3 can be also applied directly to $\tilde{\Sigma}_{\mathbf{q}}(k)$ and $\tilde{\Sigma}_{\Omega}(k)$ of Section 3.1, respectively as it is discussed in Ref. [26].

Acknowledgments

We thank O. Gunnarsson, E. Gull, J.P.F. LeBlanc, J. Merino, G. Sangiovanni, T. Schäfer and A. Toschi for useful discussions. We acknowledge financial support from the Russian Science Foundation through Grant No. 16-42-01057.

References

[1] F. Reinert, S. Hüfner, Photoemission spectroscopy – from early days to recent applications, New J. Phys. 7 (1) (2005) 97 http://stacks.iop.org/1367-2630/7/i=1/a=097.
[2] S.D. Kevan (Ed.), Angle-Resolved Photoemission: Theory and Current Applications, Elsevier Science Publisher B. V., 1992.
[3] G. Binnig, H. Rohrer, C. Gerber, E. Weibel, Surface studies by scanning tunneling microscopy, Phys. Rev. Lett. 49 (1982) 57–61, https://doi.org/10.1103/PhysRevLett.49.57.
[4] J. Hubbard, Electron correlations in narrow energy bands, Proc. R. Soc. Lond. Ser. A: Math. Phys. Sci. 276 (1365) (1963) 238–257, https://doi.org/10.1098/rspa.1963.0204 http://rspa.royalsocietypublishing.org/content/276/1365/238.abstract.
[5] T. Timusk, B. Statt, The pseudogap in high-temperature superconductors: an experimental survey, Rep. Prog. Phys. 62 (1) (1999) 61 http://stacks.iop.org/0034-4885/62/i=1/a=002.
[6] M. Uchida, K. Ishizaka, P. Hansmann, Y. Kaneko, Y. Ishida, X. Yang, R. Kumai, A. Toschi, Y. Onose, R. Arita, K. Held, O.K. Andersen, S. Shin, Y. Tokura, Pseudogap of metallic layered nickelate $R_{2-x}Sr_xNiO_4$ (R = Nd, Eu) crystals measured using angle-resolved photoemission spectroscopy, Phys. Rev. Lett. 106 (2011) 027001, https://doi.org/10.1103/PhysRevLett.106.027001.
[7] D.J. Scalapino, A common thread: the pairing interaction for unconventional superconductors, Rev. Mod. Phys. 84 (2012) 1383–1417, https://doi.org/10.1103/RevModPhys.84.1383.
[8] C. Huscroft, M. Jarrell, T. Maier, S. Moukouri, A.N. Tahvildarzadeh, Pseudogaps in the 2d Hubbard model, Phys. Rev. Lett. 86 (2001) 139–142, https://doi.org/10.1103/PhysRevLett.86.139.
[9] D. Sénéchal, A.-M.S. Tremblay, Hot spots and pseudogaps for hole- and electron-doped high-temperature superconductors, Phys. Rev. Lett. 92 (2004) 126401, https://doi.org/10.1103/PhysRevLett.92.126401.
[10] B. Kyung, S.S. Kancharla, D. Sénéchal, A.-M.S. Tremblay, M. Civelli, G. Kotliar, Pseudogap induced by short-range spin correlations in a doped Mott insulator, Phys. Rev. B 73 (2006) 165114, https://doi.org/10.1103/PhysRevB.73.165114.
[11] A. Macridin, M. Jarrell, T. Maier, P.R.C. Kent, E. D'Azevedo, Pseudogap and antiferromagnetic correlations in the Hubbard model, Phys. Rev. Lett. 97 (2006) 036401, https://doi.org/10.1103/PhysRevLett.97.036401.
[12] V.J. Emery, S.A. Kivelson, Importance of phase fluctuations in superconductors with small superfluid density, Nature 374 (6521) (1995) 434–437, https://doi.org/10.1038/374434a0.
[13] Z.A. Xu, N.P. Ong, Y. Wang, T. Kakeshita, S. Uchida, Vortex-like excitations and the onset of superconducting phase fluctuation in underdoped $La_{2-x}Sr_xCuO_4$, Nature

406 (2000) 486, https://doi.org/10.1038/35020016.
[14] Y. Wang, L. Li, M.J. Naughton, G.D. Gu, S. Uchida, N.P. Ong, Field-enhanced diamagnetism in the pseudogap state of the cuprate $Bi_2Sr_2CaCu_2O_8 + \delta$ superconductor in an intense magnetic field, Phys. Rev. Lett. 95 (2005) 247002, https://doi.org/10.1103/PhysRevLett.95.247002.
[15] Y. Kohsaka, T. Hanaguri, M. Azuma, M. Takano, J.C. Davis, H. Takagi, Visualization of the emergence of the pseudogap state and the evolution to superconductivity in a lightly hole-doped Mott insulator, Nat. Phys. 8 (2012) 534, https://doi.org/10.1038/nphys2321.
[16] V. Mishra, U. Chatterjee, J.C. Campuzano, M.R. Norman, Effect of the pseudogap on the transition temperature in the cuprates and implications for its origin, Nat. Phys. 10 (2014) 357, https://doi.org/10.1038/nphys2926.
[17] T.D. Stanescu, P. Phillips, Pseudogap in doped Mott insulators is the near-neighbor analogue of the Mott gap, Phys. Rev. Lett. 91 (2003) 017002, https://doi.org/10.1103/PhysRevLett.91.017002.
[18] M. Imada, S. Sakai, Y. Yamaji, Y. Motome, Theory of pseudogap in underdoped cuprates, J. Phys.: Conf. Ser. 449 (1) (2013) 012005 http://stacks.iop.org/1742-6596/449/i=1/a=012005.
[19] E.H. da Silva Neto, P. Aynajian, A. Frano, R. Comin, E. Schierle, E. Weschke, A. Gyenis, J. Wen, J. Schneeloch, Z. Xu, S. Ono, G. Gu, M. Le Tacon, A. Yazdani, Ubiquitous interplay between charge ordering and high-temperature superconductivity in cuprates, Science 343 (6169) (2014) 393–396, https://doi.org/10.1126/science.1243479.
[20] K.-Y. Yang, T.M. Rice, F.-C. Zhang, Phenomenological theory of the pseudogap state, Phys. Rev. B 73 (2006) 174501, https://doi.org/10.1103/PhysRevB.73.174501.
[21] T.M. Rice, K.-Y. Yang, F.C. Zhang, A phenomenological theory of the anomalous pseudogap phase in underdoped cuprates, Rep. Prog. Phys. 75 (1) (2012) 016502 http://stacks.iop.org/0034-4885/75/i=1/a=016502.
[22] R. Comin, A. Frano, M.M. Yee, Y. Yoshida, H. Eisaki, E. Schierle, E. Weschke, R. Sutarto, F. He, A. Soumyanarayanan, Y. He, M. Le Tacon, I.S. Elfimov, J.E. Hoffman, G.A. Sawatzky, B. Keimer, A. Damascelli, Order driven by Fermi-arc instability in $Bi_2Sr_{2-x}La_xCuO_{6+}$, Science 343 (6169) (2014) 390–392, https://doi.org/10.1126/science.1242996.
[23] S.I. Mirzaei, D. Stricker, J.N. Hancock, C. Berthod, A. Georges, E. van Heumen, M.K. Chan, X. Zhao, Y. Li, M. Greven, N. Barišić, D. van der Marel, Spectroscopic evidence for Fermi liquid-like energy and temperature dependence of the relaxation rate in the pseudogap phase of the cuprates, Proc. Natl. Acad. Sci. U. S. A. 110 (15) (2013) 5774–5778, https://doi.org/10.1073/pnas.1218846110.
[24] O. Gunnarsson, T. Schäfer, J.P.F. LeBlanc, E. Gull, J. Merino, G. Sangiovanni, G. Rohringer, A. Toschi, Fluctuation diagnostics of the electron self-energy: origin of the pseudogap physics, Phys. Rev. Lett. 114 (2015) 236402, https://doi.org/10.1103/PhysRevLett.114.236402.
[25] O. Gunnarsson, T. Schäfer, J.P.F. LeBlanc, J. Merino, G. Sangiovanni, G. Rohringer, A. Toschi, Parquet decomposition calculations of the electronic self-energy, Phys. Rev. B 93 (2016) 245102, https://doi.org/10.1103/PhysRevB.93.245102.
[26] O. Gunnarsson, J. Merino, T. Schäfer, G. Sangiovanni, G. Rohringer, A. Toschi, Complementary views on electron spectra: from fluctuation diagnostics to real-space correlations, Phys. Rev. B 97 (2018) 125134, https://doi.org/10.1103/PhysRevB.97.125134.
[27] T. Yoshida, X.J. Zhou, K. Tanaka, W.L. Yang, Z. Hussain, Z.-X. Shen, A. Fujimori, S. Sahrakorpi, M. Lindroos, R.S. Markiewicz, A. Bansil, S. Komiya, Y. Ando, H. Eisaki, T. Kakeshita, S. Uchida, Systematic doping evolution of the underlying Fermi surface of $La_{2-x}Sr_xCuO_4$, Phys. Rev. B 74 (2006) 224510, https://doi.org/10.1103/PhysRevB.74.224510.
[28] R.O. Jones, O. Gunnarsson, The density functional formalism, its applications and prospects, Rev. Mod. Phys. 61 (1989) 689–746, https://doi.org/10.1103/RevModPhys.61.689.
[29] G. Rohringer, A. Valli, A. Toschi, Local electronic correlation at the two-particle level, Phys. Rev. B 86 (2012) 125114, https://doi.org/10.1103/PhysRevB.86.125114.
[30] A.A. Abrikosov, L.P. Gorkov, I.E. Dzyaloshinski, Methods of Quantum Field Theory in Statistical Physics, Dover, New York, 1975.
[31] J.W. Negele, H. Orland, Quantum Many-Particle Systems, Taylor & Francis Inc., Reading, MA, United States, 1998.
[32] G.D. Mahan, Many-Particle Physics, Kluwer Academic/Plenum Publishers, New York, 2000.
[33] W. Schaich, N. Ashcroft, Theory of photoemission, Solid State Commun. 8 (23) (1970) 1959–1963, https://doi.org/10.1016/0038-1098(70)90668-X.
[34] G.D. Mahan, Theory of photoemission in simple metals, Phys. Rev. B 2 (1970) 4334–4350, https://doi.org/10.1103/PhysRevB.2.4334.
[35] G.D. Mahan, Angular dependence of photoemission in metals, Phys. Rev. Lett. 24 (1970) 1068–1070, https://doi.org/10.1103/PhysRevLett.24.1068.
[36] C. Caroli, D. Lederer-Rozenblatt, B. Roulet, D. Saint-James, Inelastic effects in photoemission: microscopic formulation and qualitative discussion, Phys. Rev. B 8 (1973) 4552–4569, https://doi.org/10.1103/PhysRevB.8.4552.
[37] J.D. Lee, O. Gunnarsson, L. Hedin, Transition from the adiabatic to the sudden limit in core-level photoemission: a model study of a localized system, Phys. Rev. B 60 (1999) 8034–8049, https://doi.org/10.1103/PhysRevB.60.8034.
[38] L. Hedin, J. Lee, Sudden approximation in photoemission and beyond, J. Electron Spectrosc. Relat. Phenom. 124 (2) (2002) 289–315, https://doi.org/10.1016/S0368-2048(02)00060-9 Frontiers in photoemission spectroscopy of solids and surfaces.
[39] A. Damascelli, Z. Hussain, Z.-X. Shen, Angle-resolved photoemission studies of the cuprate superconductors, Rev. Mod. Phys. 75 (2003) 473–541, https://doi.org/10.1103/RevModPhys.75.473.
[40] R.M. Wilcox, Bounds for the isothermal, adiabatic, and isolated static susceptibility tensors, Phys. Rev. 174 (1968) 624–629, https://doi.org/10.1103/PhysRev.174.624.
[41] J.M. Tomczak, Spectral and optical properties of correlated materials (Ph.D. thesis), Ecole Polytechnique, 2007.
[42] G. Baym, L.P. Kadanoff, Conservation laws and correlation functions, Phys. Rev. 124 (1961) 287–299, https://doi.org/10.1103/PhysRev.124.287.
[43] J.M. Luttinger, J.C. Ward, Ground-state energy of a many-fermion system, II, Phys. Rev. 118 (1960) 1417–1427, https://doi.org/10.1103/PhysRev.118.1417.
[44] R.A. Smith, Planar version of Baym–Kadanoff theory, Phys. Rev. A 46 (1992) 4586, https://doi.org/10.1103/PhysRevA.46.4586.
[45] N.E. Bickers, Theoretical Methods for Strongly Correlated Electrons, Springer-Verlag New York Berlin Heidelbert, 2004, pp. 237–296 (Chapter 6).
[46] V. Janiš, A. Kauch, V. Pokorný, Thermodynamically consistent description of criticality in models of correlated electrons, Phys. Rev. B 95 (2017) 045108, https://doi.org/10.1103/PhysRevB.95.045108.
[47] P. Hansmann, N. Parragh, A. Toschi, G. Sangiovanni, K. Held, Importance of d–p coulomb interaction for high t_c cuprates and other oxides, New J. Phys. 16 (3) (2014) 033009 http://stacks.iop.org/1367-2630/16/i=3/a=033009.
[48] T. Maier, M. Jarrell, T. Pruschke, M.H. Hettler, Quantum cluster theories, Rev. Mod. Phys. 77 (2005) 1027, https://doi.org/10.1103/RevModPhys.77.1027.
[49] A. Georges, G. Kotliar, W. Krauth, M.J. Rozenberg, Dynamical mean-field theory of strongly correlated fermion systems and the limit of infinite dimensions, Rev. Mod. Phys. 68 (1) (1996) 13, https://doi.org/10.1103/RevModPhys.68.13.
[50] G. Kotliar, S.Y. Savrasov, K. Haule, V.S. Oudovenko, O. Parcollet, C.A. Marianetti, Electronic structure calculations with dynamical mean-field theory, Rev. Mod. Phys. 78 (2006) 865, https://doi.org/10.1103/RevModPhys.78.865.
[51] K. Held, Electronic structure calculations using dynamical mean field theory, Adv. Phys. 56 (2007) 829–926, https://doi.org/10.1080/00018730701619647.
[52] I.T. Diatlov, V.V. Sudakov, K.A. Ter-Martirosian, Asymptotic meson–meson scattering theory, Sov. Phys. JETP 5 (1957) 631.
[53] G. Rohringer, H. Hafermann, A. Toschi, A.A. Katanin, A.E. Antipov, M.I. Katsnelson, A.I. Lichtenstein, A.N. Rubtsov, K. Held, Diagrammatic routes to nonlocal correlations beyond dynamical mean field theory, Rev. Mod. Phys. 90 (2018) 025003, https://doi.org/10.1103/RevModPhys.90.025003.
[54] V. Janiš, Asymptotic limit of high spatial dimensions and thermodynamic consistence of mean-field theories, Phys. Rev. Lett. 83 (1999) 2781, https://doi.org/10.1103/PhysRevLett.83.2781.
[55] K.-M. Tam, H. Fotso, S.-X. Yang, T.-W. Lee, J. Moreno, J. Ramanujam, M. Jarrell, Solving the parquet equations for the Hubbard model beyond weak coupling, Phys. Rev. E 87 (2013) 013311, https://doi.org/10.1103/PhysRevE.87.013311.
[56] G. Li, N. Wentzell, P. Pudleiner, P. Thunström, K. Held, Efficient implementation of the parquet equations: role of the reducible vertex function and its kernel approximation, Phys. Rev. B 93 (2016) 165103, https://doi.org/10.1103/PhysRevB.93.165103.
[57] T. Schäfer, G. Rohringer, O. Gunnarsson, S. Ciuchi, G. Sangiovanni, A. Toschi, Divergent precursors of the Mott–Hubbard transition at the two-particle level, Phys. Rev. Lett. 110 (2013) 246405, https://doi.org/10.1103/PhysRevLett.110.246405.
[58] V. Janiš, V. Pokorný, Critical metal-insulator transition and divergence in a two-particle irreducible vertex in disordered and interacting electron systems, Phys. Rev. B 90 (2014) 045143, https://doi.org/10.1103/PhysRevB.90.045143.
[59] G. Rohringer, New routes towards a theoretical treatment of nonlocal electronic correlations (Ph.D. thesis), Vienna University of Technology, 2013.
[60] T. Schäfer, S. Ciuchi, M. Wallerberger, P. Thunström, O. Gunnarsson, G. Sangiovanni, G. Rohringer, A. Toschi, Non-perturbative landscape of the Mott–Hubbard transition: multiple divergence lines around the critical endpoint, Phys. Rev. B 94 (2016) 235108, https://doi.org/10.1103/PhysRevB.94.235108.
[61] O. Gunnarsson, G. Rohringer, T. Schäfer, G. Sangiovanni, A. Toschi, Breakdown of traditional many-body theories for correlated electrons, Phys. Rev. Lett. 119 (2017) 056402, https://doi.org/10.1103/PhysRevLett.119.056402.
[62] P. Chalupa, P. Gunacker, T. Schäfer, K. Held, A. Toschi, Divergences of the irreducible vertex functions in correlated metallic systems: insights from the anderson impurity model, Phys. Rev. B 97 (2018) 245136, https://doi.org/10.1103/PhysRevB.97.245136.
[63] P. Thunström, O. Gunnarsson, S. Ciuchi, G. Rohringer, Analytical Investigation of Singularities in Two-Particle Irreducible Vertex Functions of the Hubbard Atom, (2018) arXiv:1805.00989.
[64] S. Liang, B. Doucot, P.W. Anderson, Some new variational resonating-valence-bond-type wave functions for the spin-1/2 antiferromagnetic Heisenberg model on a square lattice, Phys. Rev. Lett. 61 (1988) 365–368, https://doi.org/10.1103/PhysRevLett.61.365.
[65] H.W. Biester, M.J. Besnard, G. Dujardin, L. Hellner, E.E. Koch, Photoemission of pairs of electrons from rare-gas solids, Phys. Rev. Lett. 59 (1987) 1277–1280, https://doi.org/10.1103/PhysRevLett.59.1277.
[66] R. Herrmann, S. Samarin, H. Schwabe, J. Kirschner, Two electron photoemission in solids, Phys. Rev. Lett. 81 (1998) 2148–2151, https://doi.org/10.1103/PhysRevLett.81.2148.
[67] Y. Pavlyukh, M. Schüler, J. Berakdar, Single- or double-electron emission within the Keldysh nonequilibrium Green's function and Feshbach projection operator techniques, Phys. Rev. B 91 (2015) 155116, https://doi.org/10.1103/PhysRevB.91.155116.
[68] B.D. Napitu, J. Berakdar, Two-particle photoemission from strongly correlated systems: a dynamical mean-field approach, Phys. Rev. B 81 (2010) 195108, https://doi.org/10.1103/PhysRevB.81.195108.